In-beam study of ^{206}Pb level scheme including conversion electrons $\gtrsim$ 40 keV

James E. Draper, Richard J. McDonald, and Nicholas S. P. King*
Crocker Nuclear Laboratory,† University of California, Davis, California 95616
(Received 26 May 1977)

In-beam time-sorted measurements of internal-conversion electrons, γ rays, and γ-γ coincidence are reported for ^{206}Pb. The range of measurable kinetic energies of electrons was ~40–1600keV with powder targets using the reaction ^{204}Hg(α,2n)^{206}Pb. The results confirm the yrast 12+, 10+, and 9− levels in ^{206}Pb which, based on partial evidence, were tentatively proposed by the group in Stockholm. The effective quadrupole charge of the $i_{13/2}$ neutron is (0.89 ± 0.05)e. Conversion coefficients and multipolarities of 10 transitions in ^{206}Pb are reported.

[NUCLEAR REACTIONS ^{204}Hg(α, 2n), E_α = 30 MeV; measured 40–1600 keV internal conversion electron spectra, γ spectra, and γ-γ coincidence spectra in eight time bands after beam burst. Deduced levels, J, π, ICC. Si(Li) and Ge(Li) detectors.]

Many experimental observations about excited states of nuclei near ^{208}Pb have been predicted by relatively pure shell model wave functions.[1-4] This simple relationship should apply well in ^{206}Pb. Kuo and Herling[1] calculated wave functions and energies for ^{206}Pb using reaction matrix elements derived from the Hamada-Johnston potential according to the model of Kuo and Brown,[5] including the effects of core polarization. The calculation was performed in three approximations which successively added the contributions of two-hole states, 1p-3h intermediate states, and other-2h intermediate states, the latter two including core polarization. In these three approximations, the 12+$(i_{13/2})^{-2}$ state is located at 3.65, 4.34, and 4.57 MeV, respectively, above the ground state, and the 10+$(i_{13/2})^{-2}$ state is 30, 60, and 60 keV, respectively, below the 12+ state.

At about the same time as the work of Ref. 1, Bergström *et al.*[6] reported in-beam experiments on ^{204}Hg(α, 2n)^{206}Pb. They found three-γ-ray transitions (γ rays) at 458.1, 1299.1, and 1368.7 keV with half-lives of 199, 190, and 218 ns, respectively, and they proposed that within experimental uncertainties these half-lives are the same, 200 ±14 ns. Each of these γ rays had a prompt component, that of the 1369-keV γ ray being the smallest, and that of the 458-keV being the largest. Their delayed intensity balance was

$$I(1299) + I(1369) = (100 \pm 7) + (112 \pm 6)$$
$$= 212 \pm 9,$$
$$I(458) = 216 \pm 9.$$

On the basis of these data and unreported excitation functions, they proposed that the 1369-, 1299-, and 458-keV γ rays are, respectively, 12+→9−, 10+→9−, and 9−→7− transitions with the 12+ state located at 4027.2 keV and the 7− state being the 126-μs isomer at 2200 keV. These assignments were reasonably compatible with the calculations of Kuo and Herling[1] and with a report[7] that the $(i_{13/2}f_{5/2})$9− state is experimentally at 2650 keV compared to 2658 keV of Ref. 6.

However, as Bergström *et al.*[6] stated, the experimental evidence for their proposed level scheme is incomplete. They measured neither angular distributions nor internal-conversion electrons. Consequently, there was no direct evidence of the multipolarity nor the parity change involved in each transition. There was no coincidence work to establish the cascades of 1369-458 nor 1299-458 keV γ rays. The key transition, 12+→10+, had not been observed. Furthermore, any prompt component of the 1369-keV γ ray would be incompatible with their interpretation.

There has been no further experimental work to show directly that the three γ rays which Bergström *et al.* found from (α, 2n) are correctly assigned. There has been an experiment[8] in which the precession of the anisotropy of the 458-keV γ ray was measured when the target of the (α, 2n)^{206}Pb reaction was placed in a magnetic field. The purpose of that experiment was to measure the g factor of the 12+ state, but that interpretation presupposes that the 458-keV γ ray is in prompt coincidence with a transition from the 12+ state. It was argued[8] that since this interpretation gives a g factor in good agreement with previously measured g factors of $i_{13/2}$ neutrons near ^{208}Pb, the location and $(i_{13/2})^{-2}$ configuration of the 12+ state were confirmed.

Nevertheless, the 12+, 10+, 9−, and 7− structure, associated by reasonable, but incomplete,

arguments with these 1369-, 1299-, and 458-keV γ rays, should be supported by further direct experiments, and that is the purpose of the present work. This is especially true since detailed theoretical interpretations of the effective orbital g factor[8] and effective $E2$ charge[9] of the $i_{13/2}$ neutron hole have been based on this 12+, 10+, 9−, and 7− level structure. The evaluation[9] of the latter, $e^{-1}e_{\rm eff}(69.6) = 0.96 \pm 0.04$, requires not only the half-life of the 12+ state but also the branching ratio of the $E2$ 12+→10+ transition. In this regard, it is important to establish directly that there is a 69.6-keV $E2$ transition and to measure its branching ratio in order to ascertain that there is not a third strong transition from the 12+ state. Our objectives are: (1) to observe directly the missing transition from the 12+ state, *viz.*, the 12+→10+; (2) to measure, in-beam, the multipole character, including parity change, of all the transitions by measuring electron internal-conversion coefficients; (3) to determine the γ-γ coincidence relationships among the high-spin transitions.

EXPERIMENTAL METHOD

^{206}Pb was formed by the $(\alpha, 2n)$ reaction using 30-MeV α particles from the 193-cm isochronous cyclotron of the Crocker Nuclear Laboratory. The target was 93%-enriched ^{204}HgO powder deposited as a slurry by centrifuging onto 6-μm aluminized Mylar. The rather refractory HgO was ground with cleaned mortar and pestle for ~5 min in isopropyl alcohol, the material in suspension being frequently drawn off in a dropper. Then glycerine was added to the remaining HgO for further grinding and extraction. Within ~15 min virtually all of the ~1 mg HgO had been transferred. Glycerine was added to give ~50:50 alcohol:glycerine for viscosity. The mixture was stirred thoroughly, transferred to the specially constructed centrifuge tube, and centrifuged onto 6-μm aluminized Mylar at increasing speeds for ~30 min. At the highest speed the spring-loaded support for the Mylar sags, permitting the liquid to empty slowly. The target is baked at 120 °C for 15 min, then sprayed for ~2 s at 1 m with spray lacquer. The details will be published elsewhere. γ spectra were taken with a 55-cm^3 true-coaxial Ge(Li) detector at 90° to the beam direction and 9 cm from the target. Conversion-electron spectra were taken with an on-line spectrometer also at 90°. The electron spectrometer[10] consists of a solenoidal magnet, a helical Pb baffle for positron and photon shielding, and a cooled Si(Li) detector to measure energy. At room temperature the resistance of the solenoid is 1 Ω and it focuses 2000-keV electrons at 32 A. Both γ and conversion-electron events were sorted into ~8 time bands according to their arrival time compared to the 8-MHz cyclotron rf. The events were sorted and stored in the memory of an on-line PDP-15/40 computer.

γ spectra were taken over the region 60–1400 keV with an energy resolution of 3.4 keV at 1333 keV. Both energy and efficiency calibrations were made with a ^{152}Eu radioactive source using the energies and intensities of Riedinger, Johnson, and Hamilton.[11] A $\gamma_1\gamma_2 t_1 t_2$ experiment was performed to verify the 12+→···→7− part of the decay scheme. The transition γ_1 was observed in a 55-cm^3 Ge(Li) detector at ~120° from the beam, and γ_2 was observed in a 22-cm^3 Ge(Li) detector at ~45° on the same side of the beam. A Pb absorber was placed between the detectors to reduce Compton-induced coincidences. The time t_1 was the time difference between γ_1 and γ_2, and t_2 was the time of γ_2 with respect to the cyclotron rf. Data were collected via a CAMAC interface to the PDP-15/40 computer and recorded event by event on magnetic tape for off-line analysis.

The electron-collecting solenoid has an approximately Gaussian shape of transmission vs electron momentum. The full width at half maximum (FWHM) of this Gaussian curve is 0.18 of the central momentum. In order to accumulate data over a $\lesssim$30:1 dynamic range of energy, the computer sweeps the solenoid current linearly, up and down, between the limits I_1 and I_2 at 12.8 s per cycle. During each sweep of the current, the computer repeatedly calculates the upper and lower energy boundaries of the instantaneous band pass of the solenoid. It then delivers the corresponding voltages to the upper and lower discriminator levels of the swept-single-channel analyzer (SSCA) which gates the analog pulses from the Si(Li) detector. This significantly reduces the background under the spectrum.

The analyzer dead time is energy dependent since the counting rate varies significantly with electron energy and thus with solenoid current. In order to measure this dead-time correction, a logic pulse accompanying each acceptable event is stored in the appropriate channel of a 128-channel block, corresponding to the solenoid current for that event. We designate this number of pulses in a given channel as RT. Then LT is the number of pulses stored in the corresponding channel of another 128-channel block for which the logic pulses are gated off by the computer-busy or pileup-rejector signals. The ratio LT/RT is the fractional live time.

The relative efficiency of the entire system at electron energy E, when the solenoid current is swept linearly from I_1 to I_2 to I_1 an integral number of times, is $\epsilon(E)$. This is

$$\epsilon(E) = \alpha_1(E,d)(E^2+2mE)^{1/2}\alpha_2(E)\alpha_3(E)\alpha_4(E) \times \alpha_5(E)\alpha_6(E), \quad (1)$$

where $\alpha_1(E,d)$ is the fraction of electrons escaping the target of thickness d within acceptable limits of direction and energy degradation; the square root, proportional to momentum, is the averaged transmission of the solenoid; $\alpha_2(E)$ is the transmission through the 4-μm aluminized Mylar window protecting the Si(Li) detector, $\alpha_3(E)$ is the efficiency of the bare Si(Li) detector, $\alpha_4(E)$ is the efficiency of the electronic fast-timing circuitry, $\alpha_5(E)$ is the efficiency of the SSCA, and $\alpha_6(E) = (LT/RT)$ is the fractional live time of the combined analyzer and computer system. Equation (1) is valid when E is sufficiently far from E_1 and E_2, the central energies at I_1 and I_2. The quantity m is the rest energy of an electron.

Calibration data were taken with ^{152}Eu and ^{133}Ba sources thin enough that $\alpha_1(E,d) \cong 1$ for electron energies above 40 keV. The relative efficiency $\epsilon(E)$ calculated from these calibration data, using electron intensities from Malmsten *et al.*,[12] corrected by Spenny,[13] for ^{152}Eu and from Nuclear Data Sheets[14] for ^{133}Ba, followed Eq. (1) within the experimental uncertainty of ±10%. The product of α_1 through α_6 was unity over the region 45 to 1361 keV with no SSCA in the circuit. This permits assignment of $\alpha_2\alpha_3\alpha_4 = 0.95 \pm 0.05$ over this energy region, since $\alpha_6 = 1.0$ at those low counting rates.

A major problem was the absorption $\alpha_1(E,d)$ from the somewhat uneven slurry targets. Unfortunately, we could not prepare evaporated Hg targets. In such high-Z targets there can be electron attenuation out of the peak not only because of energy loss by ionization, but also because of Rutherford scattering by the nucleus.[18] For the in-beam targets we evaluated $\alpha_1(E,d)$ by the following series of measurements. Vacuum-deposited Au foils of thickness t were placed immediately over the ^{152}Eu or ^{133}Ba source and intensity losses due to scattering and absorption were measured. This gave the experimental transmission $\beta_1(E,t)$. The thickness of these Au foils was determined by x-ray fluorescence, in which the intensity of fluorescent x rays was compared to the intensity from a standard foil of known thickness. The correction was made for self-absorption of the x rays. This experimental $\beta_1(E,t)$ can be used to calculate $\alpha_1(E,d)$, where the source is assumed to be uniformly distributed in depth in the absorber, by

$$\alpha_1(E,d) = \int_0^d \beta_1(E,t)\,dt. \quad (2)$$

We assume here that the absorption and scattering in Au are the same as in Hg, and that any electron which departs the plane in which it was first emitted, while traveling in a direction at an angle $\gtrsim 90°$ from the source-detector axis, will not reach the Si(Li) detector with sufficiently small degradation of energy to be considered in the peak.

The calculation of $\alpha_1(E,d)$ requires a knowledge of the target thickness. We measured the average thickness of the HgO targets by x-ray fluorescence, as described above, and also examined each target using a surface microscope. This examination indicated that the targets were ~50–60% covered with HgO and 40–50% bare. The effective target thickness for electrons leaving the target and entering the spectrometer was calculated from the average thickness measured by x-ray fluorescence, the estimated fraction covered, and the $\sqrt{2}$ geometrical factor due to the 45° angle of the target from the spectrometer axis. The validity of this analysis was demonstrated by in-beam measurements of conversion electrons from the 142-keV $M1$ and the 147.6-keV $E2$ transitions from the 21.5-h radioactive decay of ^{200}Pb produced in a ^{198}HgO target.

The low-energy shape of $\alpha_5(E)$, for the SSCA, was measured using the Auger electrons of ^{152}Eu and $\gtrsim$30-keV electrons from a second, semithin ^{133}Ba source with and without the SSCA. The quantity $\alpha_6(E)$, fractional live time, is unity except with larger beam currents ($\gtrsim$10 nA) from the cyclotron and electron energies $\lesssim$80 keV. Table I gives these correction factors for the present data. The energy resolution of electrons was 2.4 keV full width at half maximum (FWHM) at 624 keV, but in-beam it deteriorated to ~5 keV FWHM at 50 keV owing to energy loss in escaping from various depths in the target. Time resolution was 7 ns

TABLE I. Electron efficiency correction factors in Eq. (1).

Transition	$69.7L_2$	$69.7L_3$	$69.7M_{2,3}$	$343K$	$458K$
Electron energy (keV)	54.1	56.3	66.2	256	370
$\alpha_1(E, 1.75\ \text{mg cm}^{-2})$	0.57	0.60	0.67	0.97	1.0
$\alpha_2\alpha_3\alpha_4$	0.95	0.95	0.95	1.0	1.0
α_5	0.90	0.91	0.97	1.0	1.0
α_6	0.96	0.96	0.99	1.0	1.0
$(E^2+2mE)^{1/2}$	0.24	0.25	0.27	0.57	0.72

TABLE II. Results for electron conversion. All data, except for the 1166-keV 0+→0+ transition, are from delayed bands.

Assigned transition energy (keV)	Line assignment	$(E+C)$ (keV) [a]	Energy [b] loss	Relative [c] delayed intensity	$\frac{W_\gamma(90°)}{W_{eK}(90°)}$	$10^3\alpha_k$ [d] Expt.	Theory
69.7	L	69.7	2.4	9.46 ±1.4			
	M	69.5	2.1	2.67 ±0.4			
343.5 [e]	γ	343.7		28.6 ±3	0.90		
	K	343.6	0.8	6.5 ±0.4		227 ±30	251($M1$)
	L	342.7	0.8	0.96 ±0.07			
	M	343.4	0.8	0.26 ±0.03			
458.1	γ	458.4		29.1 ±2	0.98		
	K	457.8	0.7	0.73 ±0.05		25 ±3	25($E2$)
	L	457.5	0.7	0.28 ±0.04			
516.2 [e]	γ	516.3 ±0.8		93 ±5	1.00		
	K	516.1	0.7	4.80 ±0.32		51.6 ±5	49($E3$)
	L	516.2	0.7	2.92 ±0.24			
	M	516.0	0.7	0.78 ±0.12			
537.4 [e]	γ	537.8		30.3 ±3	1.09		
	K	537.7	0.7	2.13 ±0.12		70 ±8	76($M1$)
	L	537.1	0.7	0.40 ±0.05			
803.1 [e]	γ	803.4		100 ±6	0.99		
	K	803.0	0.6	0.808 ±0.050		8.08 ±0.7	8.1($E2$)
	L	802.9	0.6	0.161 ±0.016			
	M	803.3	0.6	0.062 ±0.015			
881.0 [e]	γ	881.3		67.9 ±4	0.99		
	K	881.1	0.6	0.484 ±0.03		7.13 ±0.7	6.8($E2$)
	L	880.8	0.6	0.086 ±0.01			
1166.4	γ	···		$\lesssim 5$ [f]			
	K	1166.4	0.6	0.40 ±0.05 [f]		$\gtrsim 0.08$	···
	L	1166.1	0.6	0.067 ±0.007 [f]			
	M	···		< 0.03 [f]			
1299.4	γ	1299.4		11.4 ±1.5	1.12		
	K	1298.9	0.6	0.017 ±0.005		1.5 ±0.4	1.32($E1$)
1369.0	γ	1369.0		16.9 ±3	1.00		
	K	1369.1	0.6	0.093 ±0.01		5.5 ±1.1	6.1($E3$)
	L	1369.3	0.6	0.022 ±0.003			
	M	1369.6	0.6	0.0085 ±0.003			

[a] $C=0(\gamma)$, 88.0(K), 15.5(L), and 3.5(M). Note that the subshell ratios for each transition affect the correct L and M values of C, but that correction is not made except for the 12+→10+ for which 14.2(L) was used. The uncertainty in E_γ is ±0.5 keV except for the 516-keV γ ray. The uncertainty in electron energy is ±0.5 keV, from the peak fitting, coupled with ±0.5 mg/cm^2 in the effective target thickness as it degrades the electron energy. The listed electron energies are corrected for the energy loss as listed in the next column.

[b] The listed energy loss is that caused by 1.7 mg cm^{-2} HgO and 0.3 mg cm^{-2} of sprayed plastic, as calculated from the theory of Landau (Ref. 29).

[c] Time-integrated intensities summed over the entire time curve interpolated to exclude the additional prompt ($\lesssim$10 ns) spike.

[d] Experimental conversion coefficient α_K based on pure $E2$ for the 803-keV transition. Theoretical values are from Ref. 16.

[e] Average of energies of Refs. 21 and 22.

[f] The intensities for this prompt 0+→0+ transition are normalized to the delayed intensity of the 803-keV transition. For example, the total intensity of the 1166-keV K electron was (0.40/0.808) times the delayed intensity of the 803-keV K electron.

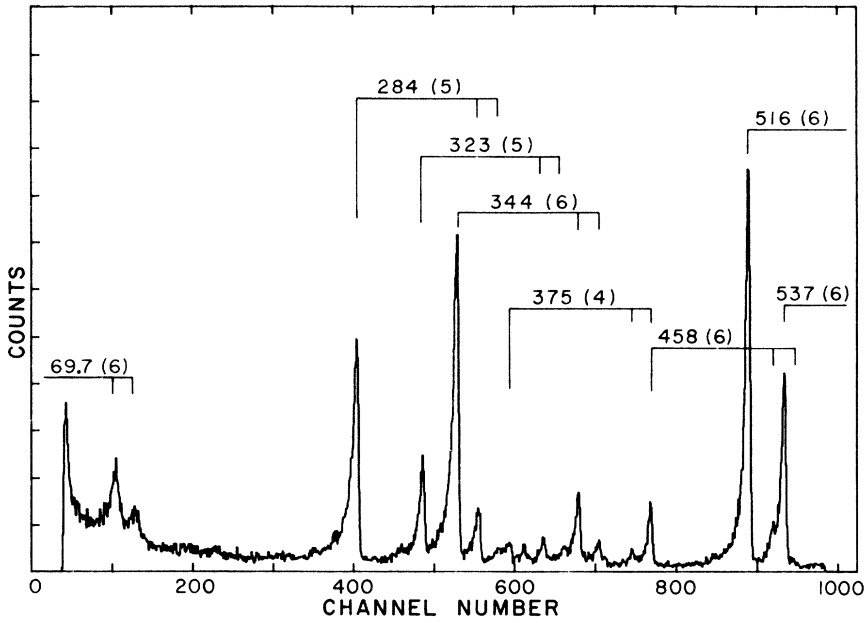

FIG. 1. Delayed, low-energy electron spectrum from $^{204}Hg(\alpha, 2n)^{206}Pb$ in the interval 41 to 101 ns after the beam burst. The first "peak" at threshold is from the timing tail of the δ rays. The transition energies are listed, and in parentheses is given the last digit of the mass number of the lead isotope—e.g., (6) is ^{206}Pb. The flags indicate K, L, and M electrons.

FWHM for 75 keV and ~13 ns FWHM for 30 keV electrons. The eight contiguous time bands covered 80–92% of the 125-ns interval between 30-MeV beam bursts in various runs. They were usually arranged with ~5-ns bands near the beam burst and progressively wider bands later, up to ~40 ns wide.

The area under each electron peak was obtained with a least-squares fit of a Gaussian joined to an exponential low-energy tail and an operator-assigned quadratic background. This program handled multiplets in which the FWHM of the Gaussian and the joining radius of the exponential tail were automatically searched for, or could be assigned, and the program determined the energies and areas of each peak. The number of peaks in a multiplet could be selected by the operator. At electron energies low enough (≲80 keV) that energy loss in the target significantly perturbed the shape, the areas were also checked by hand calculation.

Angular distributions $W_\gamma(\theta)$ and $W_e(\theta)$ are different, so this correction must be made in obtaining conversion coefficients. The initial population of m states as produced by the α particles was taken to be Gaussian. The propagation of m-state distributions through cascading transitions must also be considered. The $W_\gamma(\theta)$ and $W_e(\theta)$ were calculated using the results of Yamazaki[15] and the particle parameters of Hager and Seltzer.[16]

There is an unknown amount of relaxation of the distribution of m states due to the internal crystalline fields. This attenuation of alignment is expected to be significant in the 126-μs 7− state. The corrections for $W(\theta)$ are listed in Table II as though there were no relaxation, and that correction is not large. Relaxation will only decrease the correction, so the tabulated corrections are overestimates.

It may be of interest to note two experimental problems which delayed this work for many months. One is that after obtaining reasonable data for ^{206}Pb, although not as clean at ≲100 keV as in Fig. 1, we proceeded to obtain electron data for $^{194-204}Pb$. Later, we repeated the ^{206}Pb run, and found that the ~55-keV peaks in Figs. 1 and 2 were almost imperceptible. After considerable investigation it was found that the new Si(Li) detector, necessitated by the inability of the older one to hold bias voltage, had inadequate timing capabilities. Tests with radioactive sources showed that the two detectors had virtually the same energy resolution and time resolution, with the latter perhaps being 5–10% worse at 30 keV for the new detector. This small difference was only recognized after, in desperation, the older Si(Li) detector and potting were immersed in an ultrasonic cleaner with trichlorethylene which rejuvenated it. That 5–10% difference was crucial since the electron spectrum of Fig. 1 is in a region of time and energy where the δ rays caused by α particles colliding with electrons has been reduced by a factor ~1000, with respect to the prompt time band. This is evidenced

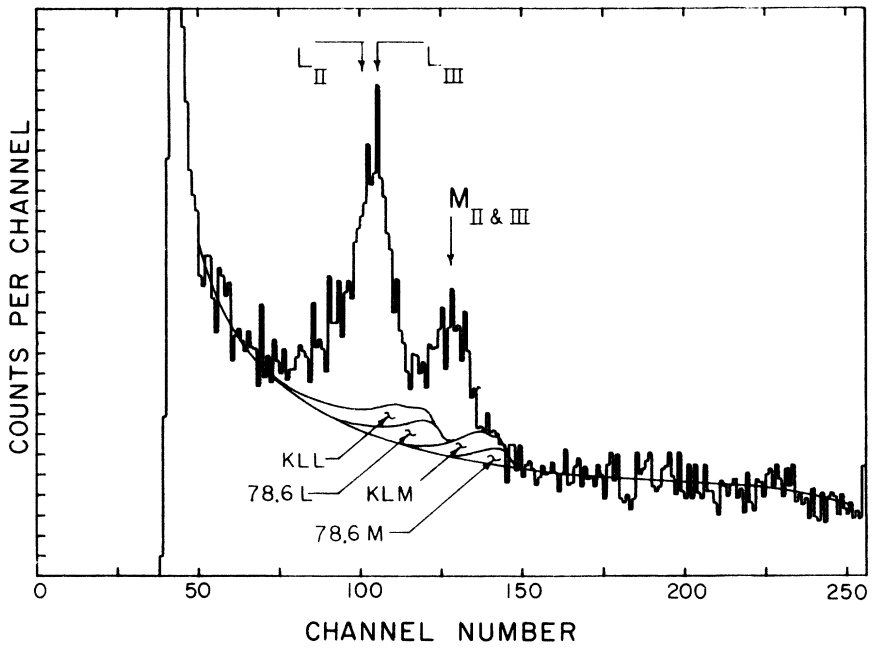

FIG. 2. The background assignments under the L and M conversion electrons from the 69.7-keV 12+ → 10+ transition in ^{206}Pb. The Auger-electron contributions and the 78.6-keV transition from ^{204}Pb are indicated.

in Fig. 3.

A kinematic analysis of a collision between a heavy projectile of mass M, kinetic energy T_α, with a light particle (electron) of mass m, kinetic energy T and bound (to an atom) with a binding energy whose magnitude is B, will show that the maximum energy T_{max} of the light particle is

$$T_{max} = (4m/M)\, T_\alpha (1 + [kBM/T_\alpha m]^{1/2}),$$

where $k = T/B$. The first factor is the result for a free stationary light particle, and the second factor is the increase caused by the fact that the kinetic energy of the struck electron increases its final energy more than the binding decreases it.

It can be shown[17] that for a perfect, zero-crossing, electronic-timing discriminator a change of 10% in the rms noise produces a factor of 3.8 in the counting rate at 10^{-3} of maximum counting rate. This caused the δ-ray spillover to obscure the ~50-keV electrons

The other experimental problem was that the intensity of the 12+→10+ transition appeared to be too small by a factor ~2. Since the efficiency of detection of in-beam 50-keV electrons can be spoiled by so many experimental factors, considerable investigation was required before it was proved that the dominant effect was Rutherford scattering of the electrons in the target,[18] as discussed above.

EXPERIMENTAL RESULTS

We have measured the L and M conversion electrons of the 70-keV $E2$ transition which deexcites the 12+ isomer in ^{206}Pb in competition with the 1369-keV $E3$ transition. Figure 1 shows the low-energy electron data. Figure 2 shows the effect of Auger electrons and the 78.6-keV transition[18] in ^{204}Pb from a 5% ^{202}Hg contaminant in the target.

The energies of the Pb Auger electrons were taken as 1.5 keV less than those of Bi, and the relative intensities were taken to be the same as those measured in Bi by Mladjenovic and Slätis.[19] The total intensity of Auger electrons was estimated by evaluating the total experimental intensities of K electrons in Fig. 4 which includes the same time bands as in Fig. 2. Using a fluorescent yield[20] of 0.96 and the estimate[20] that for Auger electrons the intensity ratio $KXY/(KLL + KLX) = 0.05$, we concluded that 4% of all K vacancies produce KLL and KLM Auger electrons.

The total intensity of the electrons from the 70-keV transition is found to equal the intensity of γ rays and electrons from the 1299-keV transition. The time distribution of the former is consistent with a half-life of 200 ns. The transition was not observed in the prompt time bands due to the large intensity of δ rays, as seen in Fig. 3.

Figures 3–5 show the conversion-electron spectra in different regions of energy and time. Figure 6 shows the γ spectra from which K-conver-

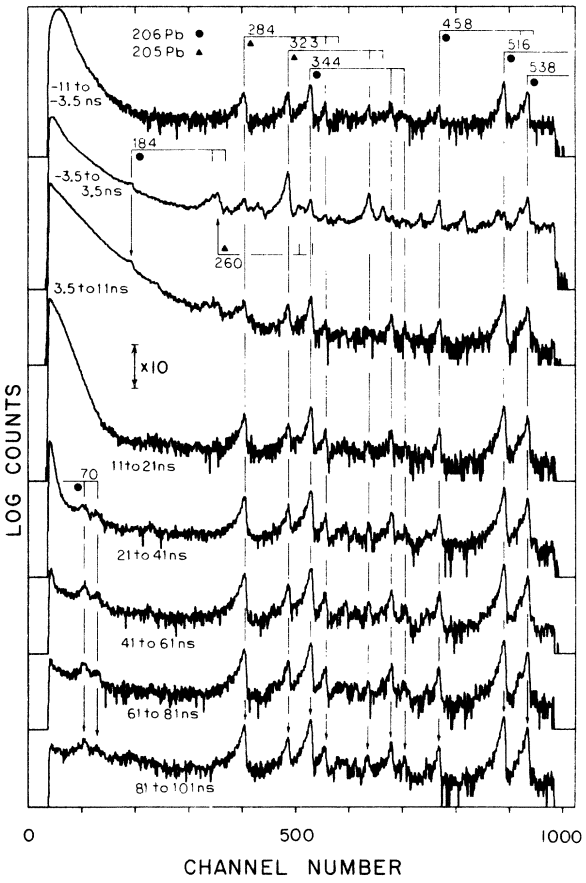

FIG. 3. Electron spectra in various time bands for 30-MeV α particles. The size of a decade for this log plot is shown. The time-band locations, with respect to the beam, are listed. This figure shows the importance of minimizing the contribution of δ rays in order to see low-energy conversion electrons.

sion coefficients were deduced. Figures 7 and 8 show the conversion coefficients. Table II summarizes the numerical results, in which the γ relative intensities are normalized to 100 for the 803-keV transition and the electron intensities are normalized to the theoretical[16] intensity for the 803-keV K line. The intensity of the 516-keV γ ray in Fig. 6 is made uncertain by the intense 511-keV γ ray. However, the results[21,22] from radioactive decay show that $\gtrsim 99\%$ of all decays of the 1684-keV state are via the 344- and 881-keV transitions, so this information was used in assigning that γ intensity and uncertainty. The experimental L/M intensity ratios give little information about the multipole character of these transitions, but they are in satisfactory agreement with theory.[16] The conversion coefficients of all transitions in Figs. 7 and 8 are compatible with essentially pure multipoles; for the transitions of interest between states of $J \leq 7$ the results from radioactive decay[21,22] show no evidence of measurable multipole admixture, i.e., <1 to 3% for various transitions.

In Table II is listed $W_\gamma(90°)/W_{eK}(90°)$, which is the factor by which an uncorrected conversion coefficient should be multiplied if the population distribution of m states were Gaussian,[15] and if that distribution were[23] $\exp[-m/(3.2+0.2J)]^2$ for the 126-μs 7− and 200-ns 12+ states. The particle parameters are from Hager and Seltzer.[16] This correction factor in Table II is maximal, applying only if there were no relaxation of this distribution under the influence of the crystalline fields of the target. For all transitions below the 126-μs state the maximum correction is small enough, and the expected relaxation large enough, that no correc-

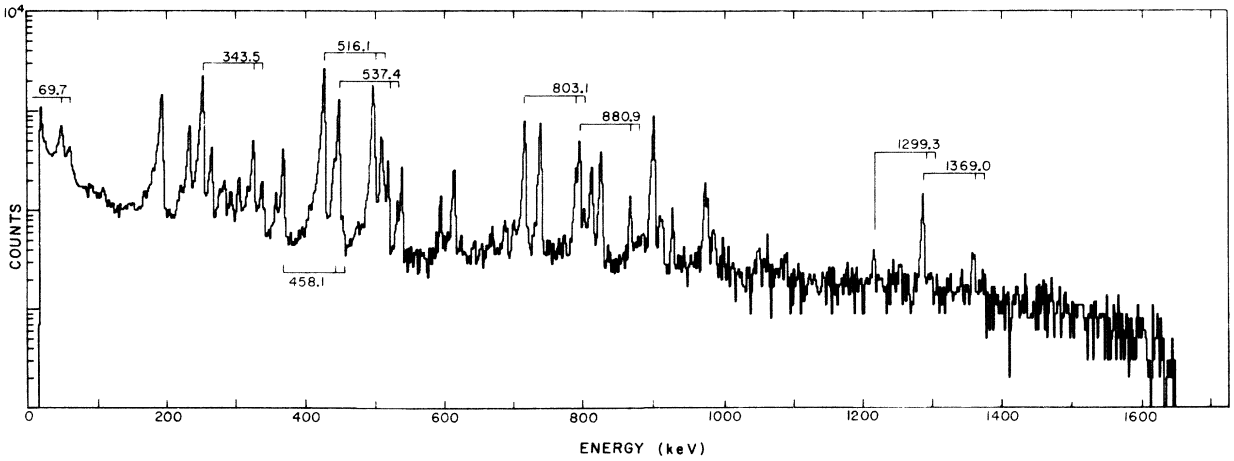

FIG. 4. Full energy range of delayed, conversion-electron spectra for transitions of interest in ^{206}Pb. This combines plots from separate low-gain and high-gain runs, joined at 470 keV. The time span is 41 to 101 ns after the beam.

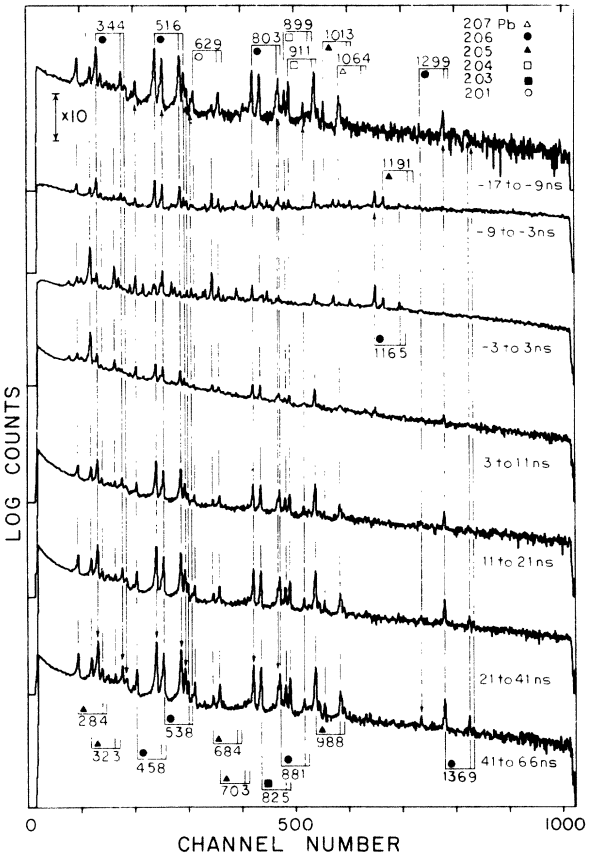

FIG. 5. Time distribution of conversion electrons through the high-energy region showing the 12+ → 9− and 10+ → 9− transitions.

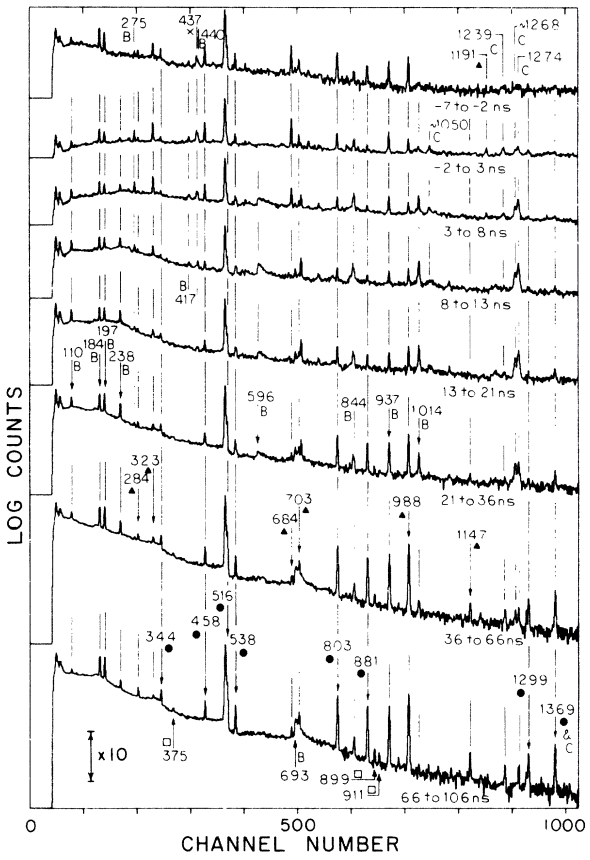

FIG. 6. Time-distribution of γ rays used in obtaining conversion coefficients.

tion was made. The only transition in Table II for which this correction may have even a small effect is the 1299-keV transition with its 12% maximum correction, and such a correction would not influence the present conclusions. Consequently, this correction was not used in the intensities of Table II.

Coincidence data are needed to provide the relationship between the 1369-, 1299-, and 458-keV transitions. Figure 9 shows the γ-γ coincidence data (22-ns resolving time) in the delayed bands. These show that the γ rays in Fig. 9(a) are in rapid cascades with the 803-keV γ rays, but the 1299- and 1369-keV γ rays are not. Similarly, Fig. 9(b) shows that only the 1299- and 1369-keV γ rays are in rapid cascades with the 458-keV γ ray. Table III gives the coincidence relations of the transitions of interest.

Figure 10 shows the level scheme of ^{206}Pb with our experimental prompt and delayed total intensities of the transitions. The prompt and delayed intensities are in satisfactory balance with each other. For the 70-keV transition $(\alpha_L + \alpha_M) = 30.6$, so this transition intensity is nearly the sum of

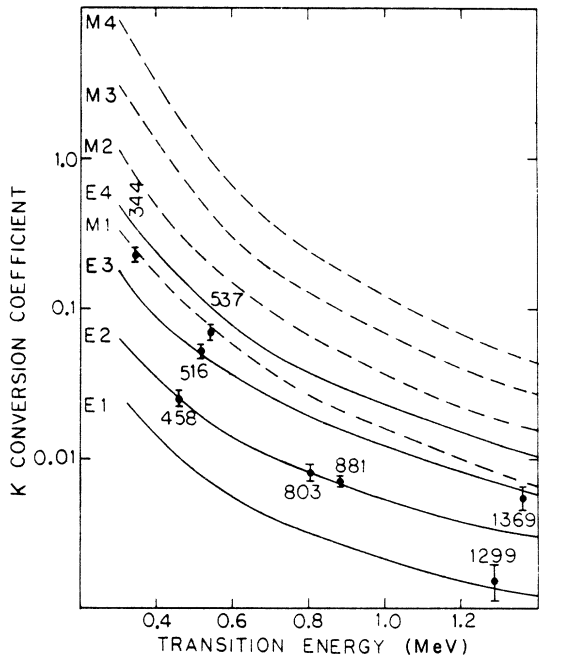

FIG. 7. K-conversion coefficients of transitions in ^{206}Pb and theoretical values from Ref. 16.

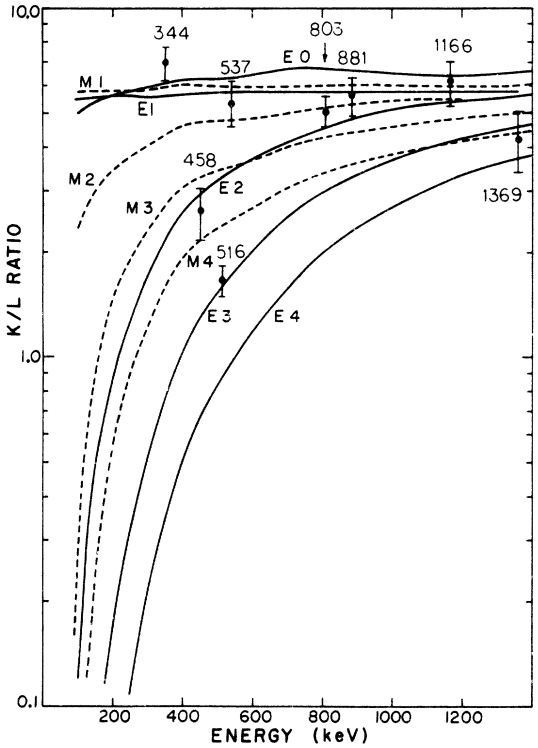

FIG. 8. Ratio of conversion coefficients from the K and L shells for ^{206}Pb.

TABLE III. Intensities of γ-γ coincidences. The symbol P denotes prompt as −6 to +6 ns after the beam; D denotes delayed, as 16 to 110 ns. Strong is S, weak is W, and A is absent.

	343	458	516	537	803	881	1299	1369
458D	A	A	A	A	A	A	S	S
803P	W	W[a]	W	S	A	S		
803D	S	A	S	W	A	S		
1299D		S						
1369D		S						

[a] This weak and uncertain coincidence would imply another 458-keV γ ray in addition to that of Fig. 10.

the electron intensities. The L/M intensity ratio is relatively insensitive to multipolarity, but its experimental value is satisfactory. The delayed intensities of the 70- and 1299-keV transitions are essentially the same. The 40% branching ratio of the 12+→10+ transition is somewhat smaller than the 49% deduced in Ref. 6. Using our results, and a total 70-keV conversion coefficient[16,24] of 32.6, to obtain the experimental $B(E2)$, and using the theoretical $\langle r^2\rangle^2$ of $i_{13/2}$ from Ref. 9 for the theoretical $B(E2)$ gives the effective $E2$ charge of this $i_{13/2}$ neutron as $(0.89\pm0.05)e$.

The recent (p,d) ^{206}Pb results[25] show the same

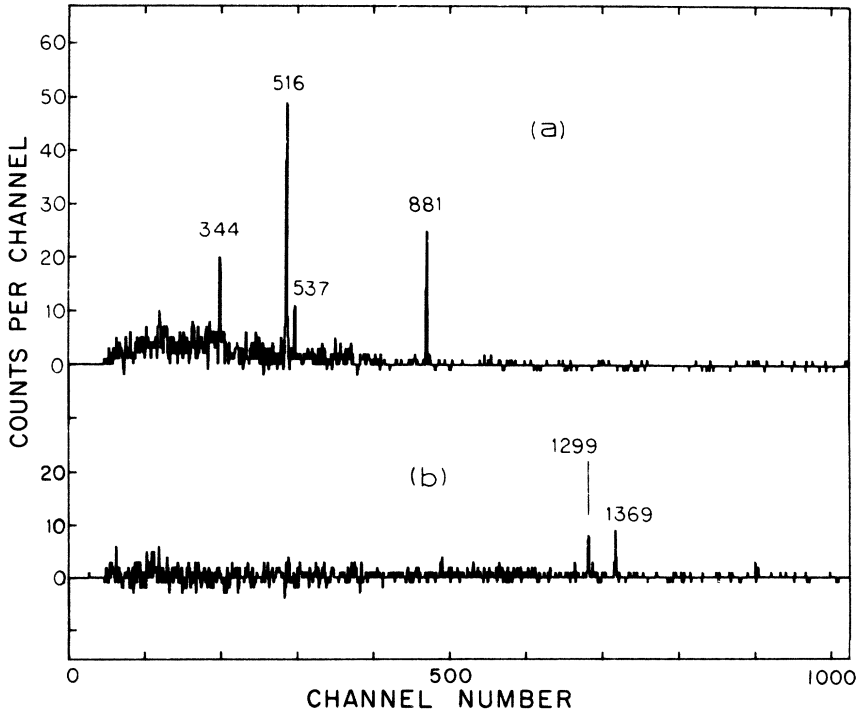

FIG. 9. Some of the γ-γ coincidence spectra. The upper spectrum is the difference between the spectrum for an 803-keV gate and the spectrum for an adjacent gate of the same width located in the background between peaks. The lower spectrum is the analogous one for a 458-keV gate. The resolving time is 22 ns. The span is 16 to 110 ns from the beam.

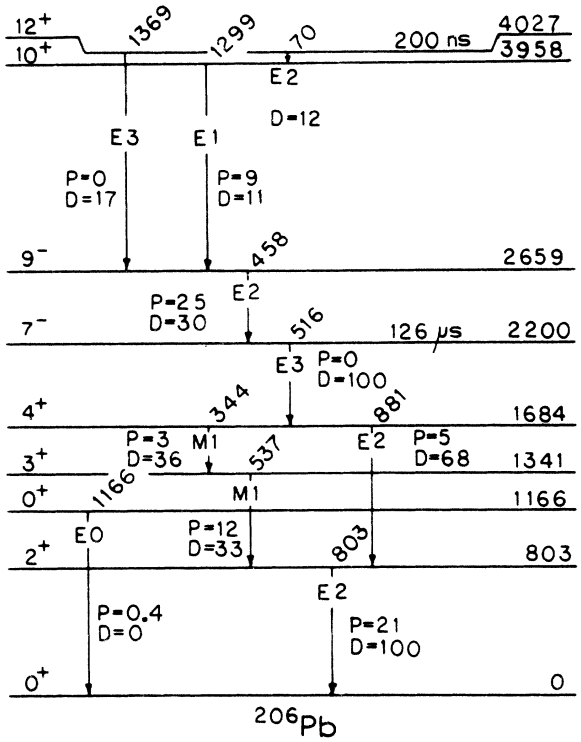

FIG. 10. Levels and transitions. The intensities labeled D are the time-integrated intensities above the interpolated delay curve, excluding the prompt spike of width $\lesssim 10$ ns. The intensities labeled P are from that prompt spike.

yrast levels as those of Fig. 10 through the 9- level at 2659 keV. The energies match to within 0.5 keV. However, the 10+ and 12+ levels require more incident angular momentum, so they were not observed in Refs. 7 and 25.

The absence of other low-energy electrons in Fig. 1 with intensity $\gtrsim 5$ and energy $\gtrsim 30$ keV shows that there are probably no gaps in the level structure of Fig. 10. This is in contrast with our results[18] in ^{200}Pb.

The half-lives of all transitions in Fig. 10 are compatible with those of Ref. 6. Since we had only 125 ns between beam bursts, while they used pulsing to obtain $\gtrsim 610$ ns between beam bursts, their half-lives are less uncertain than ours.

The K-conversion electron of the 1369 keV transition, in contrast with its γ ray, shows no prompt component, supporting the contention that it deexcites the 12+ isomer. All of the prompt intensity observed for the 1369-keV γ, and some of its delayed intensity, are due to the 1369-keV 2+→0+ transition in ^{24}Mg resulting, presumably, from neutron reactions[26] on aluminum. Data from a HgO target which did not produce ^{206}Pb were used to subtract this γ contribution, but the time distribution of the electrons is the most convincing evidence that the 1369-keV transition is only delayed.

It should be noted that the $E1$ nature of the 1299-keV transition, Figs. 7 and 8, is not possible without core excitation. Among the neutron or proton orbitals in the ^{208}Pb core there are no two with opposite parity and $\Delta j \leq 1$.

The 1166-keV $E0$ transition in Figs. 4 and 10 has been discussed in Refs. 27 and 28. There is no evidence in Fig. 6 for a 1166-keV γ ray. Our upper limit on that γ intensity gives $\alpha_K \gtrsim 0.08$, in excess of α_K for $M4$. The half-life implied in Fig. 5 is <6 ns, and in Ref. 28 it is measured to be 0.97 ns. This combination of large α_K and short half-life require it to be $E0$. The (p,d) work[25] gives a 0+ state at 1167 keV. The relative yield of this 0+ state here is so weak that we are unable to reduce the upper bound on the 0+→2+ branching ratio from the value of $\frac{1}{60}$ given in Ref. 27. Our experimental $K/L/M$ ratio is $(6.0\pm1)/1/(<0.5)$ in satisfactory agreement with the theoretical[16,30] values 5.77/1/0.3.

*Present address: Los Alamos Scientific Laboratories, Los Alamos, New Mexico 87545.

†Work supported in part by National Science Foundation.

[1]T. T. S. Kuo and G. H. Herling, NRL Report No. 2258, 1971 (unpublished).

[2]J. Vary and J. N. Ginnochio, Nucl. Phys. A166, 479 (1971).

[3]C. W. Ma and W. W. True, Phys. Rev. C 8, 2313 (1973), and references therein.

[4]C. M. Ko, T. T. S. Kuo, and J. B. McGrory, Phys. Rev. C 8, 2379 (1973).

[5]T. T. S. Kuo and G. E. Brown, Nucl. Phys. 85, 40 (1966).

[6]I. Bergström, J. Blomqvist, B. Fant, A. Filevich, G. Lindén, K.-G. Rensfelt, J. Sztarkier, and K. Wikström, Phys. Scr. 3, 11 (1971).

[7]S. M. Smith, P. G. Roos, A. M. Bernstein, and C. Moazed, Nucl. Phys. A158, 497 (1970).

[8]K. Nakai, B. Herskind, J. Blomqvist, A. Filevich, K.-G. Rensfelt, J. Sztarkier, I. Bergström, and S. Nagamiya, Nucl. Phys. A189, 526 (1972).

[9]G. Astner, I. Bergström, J. Blomqvist, B. Fant, and K. Wikström, Nucl. Phys. A182, 219 (1972).

[10]W. W. Wyckoff and J. E. Draper, Phys. Rev. C 8, 796 (1973).

[11]L. L. Riedinger, N. R. Johnson, and J. H. Hamilton, Phys. Rev. C 2, 2358 (1970).

[12]G. Malmsten, O. Nilsson, and I. Andersson, Ark. Fys. 33, 361 (1966).

[13]D. L. Spenny, Ph.D. thesis, 1970, University of Colora-

do, Boulder, Colorado (unpublished), University Microfilms Order No. 71-5933.
[14]E. A. Henry, Nucl. Data Sheets 11, 497 (1974).
[15]T. Yamazaki, Nucl. Data A3, 1 (1967).
[16]R. S. Hager and E. C. Seltzer, Nucl. Data A4, 1 (No. 1, 2) (1968); A4, 397 (No. 5, 6) (1968); A6, 1 (No. 1) (1969).
[17]J. E. Draper, Nucl. Instrum. Methods 136, 151 (1976); and (unpublished).
[18]J. E. Draper and R. J. McDonald (unpublished).
[19]M. Mladjenovic and H. Slätis, Ark. Fys. 9, 41 (1954).
[20]I. Bergström and C. Nordling, in *Alpha-, Beta- and Gamma-Ray Spectroscopy* (North-Holland, Amsterdam, 1965), p. 1535.
[21]J. C. Manthuruthil, D. C. Camp, A. V. Ramaya, J. H. Hamilton, J. J. Pinajian, and J. W. Doornebos, Phys. Rev. C 6, 1870 (1972).
[22]M. Kanbe, M. Fujioka, and K. Hisatake, Nucl. Phys. A192, 151 (1972).
[23]J. E. Draper and R. M. Lieder, Nucl. Phys. A141, 211 (1970).
[24]O. Dragoun, Z. Plajner, and F. Schmutzler, Nucl. Data A9, 119 (1971).
[25]W. A. Lanford and G. M. Crawley, Phys. Rev. C 9, 646 (1974).
[26]R. L. Bunting and J. J. Kraushaar, Nucl. Instrum. Methods 118, 565 (1974).
[27]H. C. Griffin and A. M. Donne, Phys. Rev. Lett. 28, 107 (1972).
[28]J. W. Tape, E. G. Adelberger, D. Burch, and L. Zamick, Phys. Rev. Lett. 29, 878 (1972).
[29]G. Knop and W. Paul, *Alpha-, Beta- and Gamma-Ray Spectroscopy* (see Ref. 20), p. 13.
[30]E. L. Church and J. Weneser, Phys. Rev. 103, 1035 (1956).